

LETTER

Open Access



Investigation of LIG-based pressure sensors with various silicon-based elastomeric encapsulation layers

Yoo-Kyum Shin¹, Ki-Hoon Kim¹ and Min-Ho Seo^{1,2*}

Abstract

Laser-induced graphene (LIG) has attracted significant interest in the field of pressure sensors owing to the high sensitivity associated with its inherent three-dimensional porous structure. However, the brittleness of fabricated LIG poses a critical challenge in terms of durability. To address this issue, current research on LIG-based pressure sensors has focused on the utilization of Si-elastomer encapsulation layers. Despite the importance of the mechanical properties of Si elastomers for the performance of physical sensors, few studies have been conducted on the characterization of pressure sensors based on the encapsulation layer. In this study, we investigated the electromechanical characteristics of LIG-based pressure sensors encapsulated in various Si-based elastomers. For an unbiased evaluation, we first introduce a simple and reliable fabrication process for LIG-based pressure sensors with different Si-elastomer encapsulation layers. Subsequently, the electromechanical responses of the sensors were characterized using an automated pressure machine, demonstrating that sensors with encapsulation layers with a lower Young's modulus exhibited increased resistance changes and extended response times. Finally, an in-depth exploration of the environmental stability of the pressure sensors was conducted for various encapsulation materials, ultimately confirming negligible performance variations based on the encapsulation materials.

Keywords LIG (laser-induced graphene), Pressure sensor, Elastomeric encapsulation layer

Introduction

Laser-induced graphene (LIG) is a three-dimensional (3D) porous graphene material that is synthesized by irradiating a polyimide (PI) film with a CO₂ laser in an atmospheric environment [1, 2]. The LIG-fabrication process offers significant advantages in terms of simplicity, throughput, cost-effectiveness, and scalability, eliminating the need for complex and expensive facilities, such

as clean rooms [3]. The resulting 3D graphene structure exhibits a high surface-to-volume ratio, making it highly desirable for various applications, including biosensors [4, 5], chemical sensors [6, 7], gas sensors [8–10], and catalysts [11, 12]. Among their diverse applications, LIG-based electrical-type physical sensors have garnered considerable attention because of their remarkable sensitivity [13, 14]. Particularly, LIG-based pressure sensors demonstrate exceptional sensitivity owing to the inherent deformability of the 3D graphene structure, which undergoes significant structural changes, even under minimal pressure, leading to considerable variations in electrical resistance. Thus, studies have actively utilized LIG-based physical (or pressure) sensors for various low-pressure-measurement applications.

Although LIG-based pressure sensors are highly sensitive, they are limited by durability issues. The 3D porous

*Correspondence:

Min-Ho Seo
mhseo@pusan.ac.kr

¹ Department of Information Convergence Engineering, Pusan National University, 49 Busandaehak-ro, Mulgeum-eup, Yangsan-si, Gyeongsangnam-do 50612, Republic of Korea

² School of Biomedical Convergence Engineering, Pusan National University, 49 Busandaehak-ro, Mulgeum-eup, Yangsan-si, Gyeongsangnam-do 50612, Republic of Korea

structure of the brittle carbon nanomaterial that generates LIG can easily lead to the exfoliation, fracture, and plastic deformation of the LIG nanostructure when exposed to external mechanical stimuli [15]. To address this durability issue, current research on LIG-based pressure sensors uses encapsulation layers. For example, by laminating additional films such as polymethyl methacrylate tape and Kapton tape on LIG [13, 16], the exfoliation of the LIG structure was suppressed by the applied physical stimulation. However, plastic deformation and fracture of LIG are inevitable, even under the developed laminated film; thus, the reliability of LIG for physical sensors is not confirmed.

More recently, studies have employed curable Si-based elastomers, such as polydimethylsiloxane (PDMS), as an alternative passivation layer [15, 17]. By pouring a liquid elastomer onto the LIG and subsequently applying a curing process, the elastomer can create a uniform and compact coating on the LIG, similar to a composite structure. This coating significantly enhanced the durability of LIG against mechanical pressure because the elastomer supported the LIG against mechanical pressure. Despite the significant interest in the elastomer-coating method, few studies have investigated the electromechanical characteristics of LIG-based sensors based on different encapsulation elastomers. Herein, we investigate the electromechanical characteristics of LIG-based pressure sensors with encapsulation layers composed of Si-based elastomers, specifically PDMS and Ecoflex, which possess distinct mechanical properties. For an unbiased evaluation, we first introduce a simple and reliable fabrication process designed to isolate the influence of different elastomer encapsulation layers on LIG-based pressure sensors. Using this method, various LIG-based pressure sensors with different elastomer encapsulation layers are fabricated. Subsequently, we conduct a comprehensive electromechanical characterization of these pressure sensors using an automated pressure machine to evaluate their performance in terms of electrical-resistance response, response time, long-term reliability, and stability.

Results and discussion

We developed a simple and reliable fabrication process based on spin-coating to objectively evaluate the effects of different elastomer encapsulation layers on LIG-based pressure sensors (Fig. 1). First, a PI film with two separated metal electrodes (Cu) on its surface was prepared using a conventional printed-circuit-board process. The LIG, which was the sensing part of the pressure sensor, was fabricated by irradiating a CO₂ laser on the PI film. We used scanning electron microscopy (SEM), Raman spectroscopy, and 3D optical microscopy to confirm

the high quality of the fabricated porous 3D LIG (thickness $\approx 80 \mu\text{m}$) (Additional file 1: Fig. S1, S2). Despite the fabrication processes used for the electrode and LIG, the interface between the two parts was not mechanically or electrically interconnected (Additional file 1: Fig. S2); thus, we connected the LIG and metal electrodes using a small amount of silver paste (Additional file 1: Fig. S3). Notably, we can neglect the contact resistance between the LIG and Cu electrode because the Ag paste makes conformal contact between the LIG and Cu electrode, and the LIG is also formed to have a serpentine structure in the middle (width = 300 μm , length = 107.9 mm), dominating the total resistance. Next, a liquid-phase elastomer was deposited on the LIG pressure-sensor structure using a spin coater. In this step, we utilized various elastomer layers, such as PDMS 5:1, PDMS 10:1, PDMS 20:1, and Ecoflex 1:1, by varying the ratio of the base to the curing agent to control the mechanical properties of the encapsulation layer after curing. The thickness of the elastomer layer was standardized to $\sim 180 \mu\text{m}$ via the spin-coating process. The specimens were then placed in a vacuum chamber to remove air from the porous region of the LIG while filling the elastomer (Additional file 1: Fig. S4). Finally, the encapsulation layer was cured by heat treatment using a hot plate, and enamel-coated Cu wire was soldered onto the metal electrodes for measurement. Details of the fabrication conditions are included in the Methods section.

Visual inspection of the fabricated devices was performed using optical microscopy and SEM. Optical microscopy images revealed negligible structural deformation or fractures within the LIG pattern, Ag interconnections, and Cu electrode, even after the entire process (Fig. 2A). Subsequently, a cross-sectional analysis of the device was conducted using SEM. At lower magnifications, the SEM images exhibited complete and conformal coverage of the LIG by the encapsulated PDMS layer (Fig. 2B). Additionally, at higher magnifications, the SEM images confirmed the impeccable filling of the 3D LIG structure with elastomeric material, thereby eliminating any porosity and enabling enhanced mechanical durability under applied pressure (Fig. 2C).

Before its evaluation as a pressure sensor, a basic electrical characterization of the fabricated device was performed to confirm the fabrication reliability. A current-voltage (I-V) measurement of the fabricated sensor confirmed that the sensor formed an ohmic contact within a range of -3 – 3 V (Fig. 2D). Notably, the negligible change of the I-V curves measured before and after encapsulation verified that the encapsulation process had little influence on the structural and electrical properties (Additional file 1: Fig. S5). The reproducibility of the proposed process was also confirmed. Thirteen different

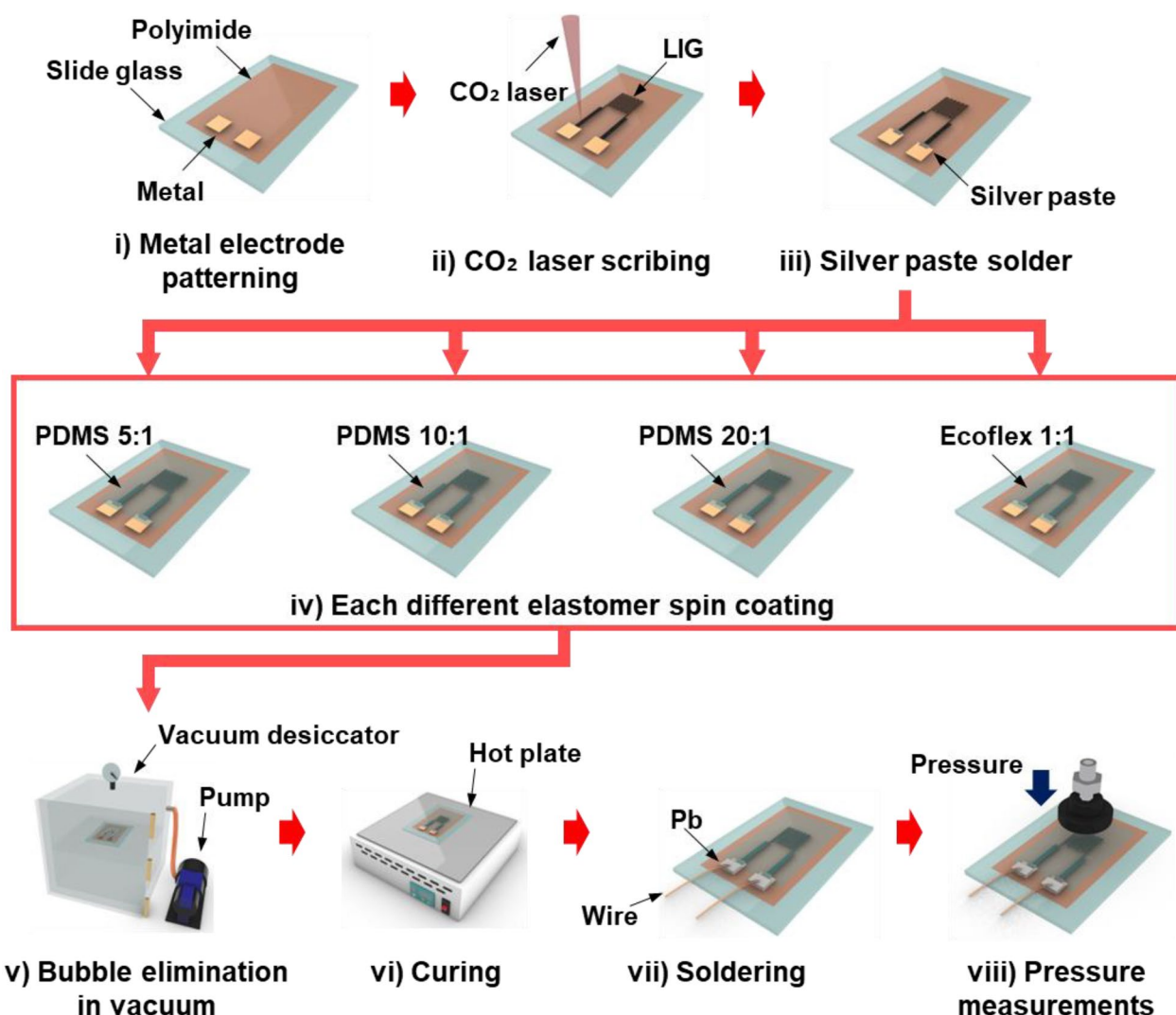


Fig. 1 Steps for fabricating LIG-based pressure sensor. **i** The formation of a metal electrode on the polyimide. **ii** The formation of LIG using a CO₂ laser. **iii** The silver-paste soldering between the metal and LIG. **iv** The encapsulation of the device using various elastomers (PDMS 5:1, 10:1, 20:1, and Ecoflex 1:1) via spin coating. **v** The bubble elimination in vacuum. **vi** The curing of the elastomer. **vii** The connection between pad and wire using Pb solder. **viii** Pressure measurements of sensors

sensors were fabricated under the same conditions, and their resistances were compared, confirming an average of 9.67 kΩ. Considering a deviation of 0.47 kΩ (4.86%), the proposed process exhibited high reproducibility, indicating that it is a reliable process for fabricating sensor devices and fairly evaluating the electromechanical characteristics of the sensors (Fig. 2E).

Next, we evaluated the electromechanical characteristics of the LIG-based pressure sensors with different encapsulation layers. For an unbiased evaluation, mechanical pressure was applied to the LIG serpentine structure using an automated force gauge (M5-20, Mark-10, USA), and the resistance of the sensor was

simultaneously acquired using a source meter (B2902A, Keysight, USA) (Fig. 3A). First, we measured the change in the electrical resistance of the PDMS 20:1 fabricated sensor based on the applied pressure. When different pressures of 100, 200, 300, and 400 kPa were applied to the sensors, the sensors showed a noticeable and reproducible increase in electrical resistance (Fig. 3B), and as the applied pressure increased, the resistance increased consistently. We consider that these results are owing to the reduction of the electrical-path area by mechanical pressure. When pressure was applied, the thickness of the 3D LIG decreased owing to structural compression, hindering electrons from traveling through the conductive

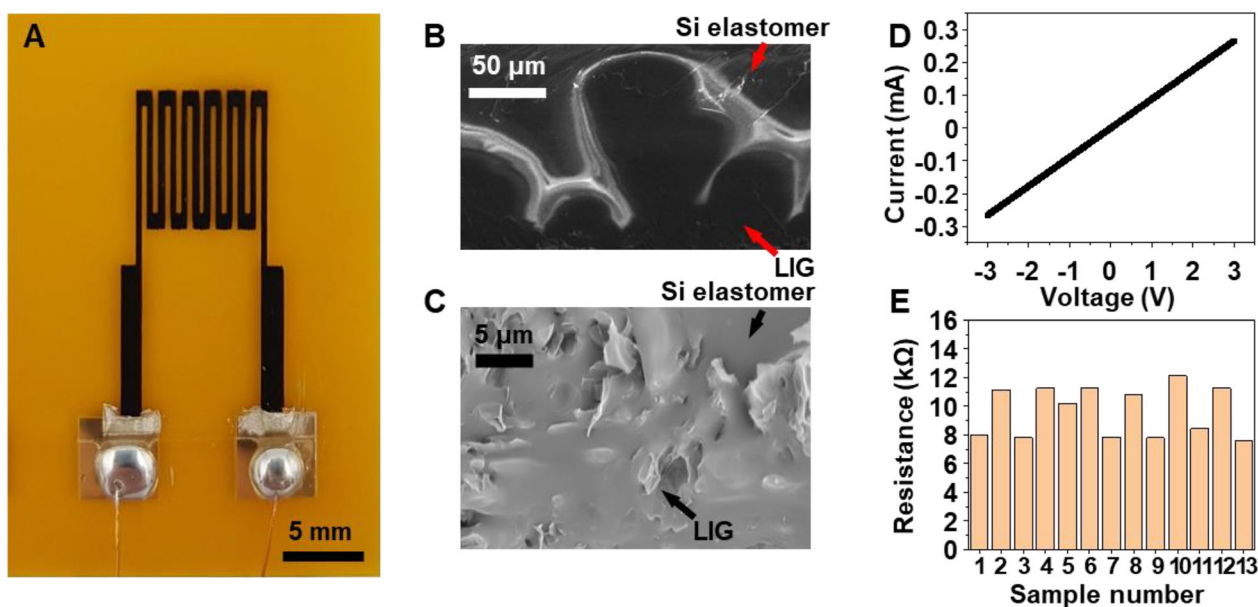


Fig. 2 Fabrication result and piezoresistive initial result. **A** Photograph of a fabricated LIG-based pressure sensor. **B** SEM image and **C** magnified SEM image of cross-sectional view of the LIG/Si elastomer composite. **D** Measured IV curve. **E** Raw data of resistance values for LIG-based pressure sensors

area (Fig. 3C). The change in the dynamic resistance of the fabricated sensors was measured to confirm their dynamic response (Fig. 3D). When no pressure was applied, the sensor did not exhibit changes in resistance. However, when pressure was applied, the sensor showed noticeable resistance changes with a trend similar to that of the applied pressure. After maintaining the change in resistance, the sensor exhibited a decrease in resistance with a similar trend as the applied force was removed (Fig. 3E). To experimentally confirm the influence of the different encapsulation layers on the pressure-sensor performance, we conducted the same experiment on all the fabricated devices and extracted the static and dynamic electrical responses with respect to the applied pressure. Notably, the resistance increased consistently across the devices, indicating the same operational mechanism as the applied pressure.

We quantitatively evaluated the electromechanical characteristics of the encapsulation layers of various materials by quantitatively extracting the resistance changes of the fabricated sensors under various pressures ranging from 10 to 400 kPa (Fig. 3F). The plot of resistance change versus applied pressure confirms that all devices show a consistent increase in resistance as the applied pressure increases; however, the change in the device made of Ecoflex is the most significant. At 400 kPa, the measured electrical resistance changes were 0.241%, 0.187%, 0.018%, and 0.011% for devices encapsulated by Ecoflex and PDMS 20:1, 10:1, and 5:1, respectively. We

consider that the trend of this result is associated with the Young's modulus of the encapsulation material, owing to the proposed resistance-change mechanism. To confirm the Young's moduli of the encapsulation-layer materials, we fabricated dog-bone model structures for each elastomer and conducted tensile tests using a force gauge (M5-2, Mark-10, USA) (Additional file 1: Fig. S6). Stress-strain curves were plotted for the dog-bone structures of PDMS 5:1, PDMS 10:1, PDMS 20:1, and Ecoflex 1:1 using the force gauge, and the Young's moduli were measured. PDMS 5:1, PDMS 10:1, PDMS 20:1, and Ecoflex 1:1 have Young's moduli of 1.75 ± 0.1 MPa, 1.136 ± 0.019 MPa, 0.37 ± 0.034 MPa, and 0.073 ± 0.002 MPa, respectively, which are in good agreement with the trend of the resistance change. Details of the Young's-modulus evaluation are included in the Additional file 1: Fig. S6, and Table S1.

The response times of the devices were also investigated. To measure this, we subjected all the fabricated sensors to pressures ranging from 100 to 400 kPa (Fig. 3G). For the evaluation, the response time was defined as the duration required for the resistance change to reach 10–90% of the total resistance change. Based on the resistance change versus applied pressure plot, we observed a consistent increase in the response time as the applied pressure increased for all devices. This test confirmed that the PDMS 5:1 encapsulation material exhibited a rapid response. Specifically, at 100 kPa, the measured response times were 505 ms, 746 ms, 811 ms, and 861 ms for the devices encapsulated with PDMS

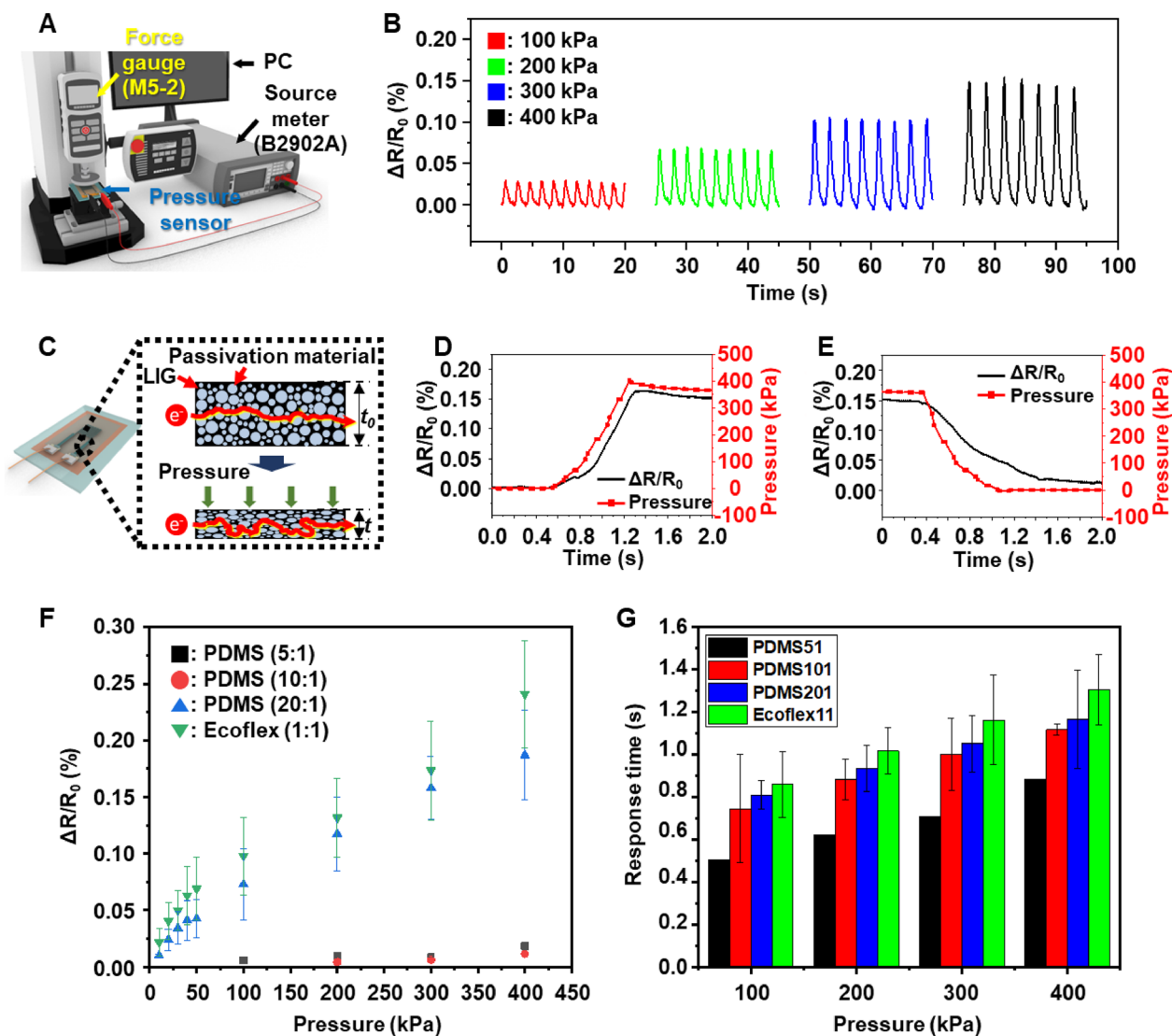


Fig. 3 Piezoresistive test and analysis. Schematic of **A** the pressure-measurement setup. **B** Relative resistance change with applied pressure for the pressure sensor. **C** Schematic of the principle of the LIG-based pressure sensor. **D** Response time and **E** recovery time of the pressure sensor with PDMS 20:1 encapsulation under 400 kPa. **F** Relative resistance change with applied pressure for pressure sensors with a Si-elastomer-based material as encapsulation (PDMS 5:1, 10:1, 20:1, and Ecoflex 1:1; N = 3). **G** Response time of the pressure sensors with various encapsulations (PDMS 5:1, 10:1, 20:1, and Ecoflex 1:1) under 100, 200, 300, and 400 kPa

5:1, PDMS 10:1, PDMS 20:1, and Ecoflex 1:1, respectively. We also attribute this response-time trend to the Young’s modulus of the encapsulation material. A higher Young’s modulus results in a smaller change in thickness under the same pressure, thereby requiring less time to achieve the maximum resistance change [18].

The mechanical stabilities of various encapsulation layers were evaluated through cyclic operations. Pressure sensors with different encapsulation layers were

tested by repeatedly applying a pressure of 400 kPa, which resulted in a resistance-change measurement during cycling. Initially, the devices fabricated with Ecoflex and PDMS 20:1 exhibited sensitivities that were 5.3 times higher than those of devices fabricated with PDMS 5:1 and 10:1. These results can be interpreted as the result of the high applied strain owing to the low Young’s modulus. However, the resistance changes of the devices fabricated with Ecoflex and

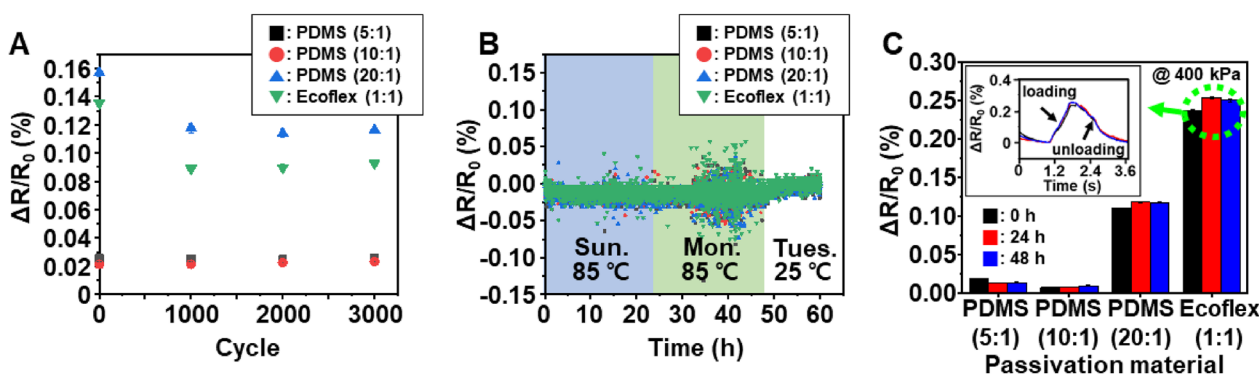


Fig. 4 Results of repeatability test and accelerated-degradation test. **A** Results of repeatability test for approximately 3000 cycles. Accelerated-degradation test results of **B** relative resistance change as a function of time and **C** sensors with various encapsulation materials (N=3)

PDMS 20:1 decreased initially in the first 1000 cycles, but remained stable after 1000 cycles (Fig. 4A). This was attributed to graphene inside the pressure sensor undergoing permanent deformation because of the large deformation and stabilization within 1000 cycles. However, the resistance changes of the devices were saturated, and even after applying pressure more than 3000 times during the cyclic test, an inconspicuous degradation in the sensor performance was confirmed in all sensors (Additional file 1: Fig. S7). Specifically, the resistance change was measured to be 0.025%, 0.021%, 0.117%, and 0.089% for PDMS 5:1, PDMS 10:1, PDMS 20:1, and Ecoflex 1:1, respectively. In the cases of PDMS 20:1 and Ecoflex, degradation in the initial characteristics was observed, but these sensors still showed a high level of change in their response characteristics. The mechanical stability test indicated that the pressure sensor for an encapsulation with a low Young's modulus requires suitable initial stabilization at high pressures.

The environmental stabilities of these devices were also tested. Accelerated-degradation tests were conducted by continuously measuring base resistance changes of the fabricated pressure sensors with different elastomer-based encapsulation layers in an 85 °C oven (Additional file 1: Fig. S8). Despite being continuously exposed to the 85 °C environment for 48 h, no significant resistance change was confirmed (Fig. 4B). Some minor fluctuations were observed in the data; however, these were believed to be the result of noise from the surrounding environment. For quantitative analysis, we extracted the resistance change of the device with mechanical pressure over time. The results show that the fabricated pressure sensors with different elastomer-based encapsulation layers, which were heated before testing for 24 and 48 h, exhibited no

significant degradation in their electrical resistance change at 400 kPa pressure. The response characteristics of the pressure sensors were maintained when the pressure was loaded and unloaded from the sensors (Fig. 4C).

Summary and conclusion

This study investigated the effects of the mechanical properties of elastomers on the characteristics of LIG-based pressure sensors utilizing an encapsulation layer. To achieve this, we proposed a simple and reliable fabrication process that utilized different elastomer materials as encapsulation layers to measure the electromechanical characteristics of LIG-based pressure sensors. The fabricated devices exhibited ohmic contact and had 9.67 ± 0.47 k Ω of resistance. The resistance of the fabricated LIG-based pressure sensors with the encapsulation layers increased when pressure was applied. We confirmed that as the Young's moduli of the encapsulation materials decreased, the resistance change increased, and the response time increased. Moreover, through repeated cycling and accelerated-degradation tests, we confirmed that the stabilities of the LIG-based pressure sensors with the encapsulation layers were not significantly compromised, even when a flexible material was used. Based on these results, we expect that adjusting the Young's modulus of the encapsulation-layer material of LIG-based pressure sensors according to the application can control changes in their resistance and response time.

Method

Sensor fabrication A CO₂ laser (BG-GRC 6040B-RD 80 W, BUGWANG GTC, Republic of Korea) was used to irradiate the PI film with a Cu electrode at a power of 11.2 W and scan speed of 250 mm/s. The resulting LIG had a uniform

thickness of approximately 80 μm . A silver paste (Two Part Conductive Silver Paint, Electron Microscopy Sciences, USA) was then applied between the LIG and Cu electrode and cured at 100 $^{\circ}\text{C}$ for 30 min. Then, spin coating was performed for 30 s at 500 rpm to form a uniform protective layer with a thickness of approximately 180 μm . Four different elastomers with different ratios were used to form the protective layers: PDMS 5:1 (Sylgard 184 silicone elastomer), PDMS 10:1, PDMS 20:1, and Ecoflex 1:1 (EcoflexTM 00–30). To remove the bubbles inside the LIG and fill the porous structure with an elastomer, the device was placed in a vacuum desiccator and subjected to vacuum treatment using a vacuum pump for 30 min. The elastomer inside the device was cured for 2 h at 80 $^{\circ}\text{C}$ on a hot plate (NEO HOTPLATE HI-1000, AS ONE, Japan).

Supplementary Information

The online version contains supplementary material available at <https://doi.org/10.1186/s40486-023-00176-9>.

Additional file 1: Figure S1. Confirmation of porous LIG based on **a** SEM image and **b** Raman spectrum analysis. **Figure S2.** 3D images of LIG and metal electrode. **Figure S3.** Optical microscopy image of interconnection between LIG and metal electrode **a** after irradiating CO₂ laser and **b** after silver-paste soldering. **Figure S4.** Bubble elimination. **a** Vacuum treatment, **b** after vacuum treatment. **Figure S5.** IV curve before/after elastomer passivation. **Figure S6.** Results of stress-strain measurements and Young's moduli of different elastomers. Schematics of **a** the fabricated dog-bone model and **b** tensile test set-up. **c** Stress-strain curve of different elastomers. **d** Young's moduli of different elastomers. **Figure S7.** Results of repeatability test **a** over 3000 cycles and **b** for 0, 1500, and 3000 cycles. **Figure S8.** Accelerated-degradation test. **a** Photograph of experimental set-up. **b** Circuit for resistance measurement. **c** Base resistance for accelerated-degradation test. **Table S1.** Mechanical properties of different elastomers.

Acknowledgements

This work was supported by a 2-year research grant of Pusan National University.

Author contributions

YKS: conceptualization, figure preparation, experiment design, data analysis, writing—original manuscript; KHK: Data analysis; MHS: methodology, supervision, writing—review and editing. All the authors have read and approved the final version of the manuscript.

Funding

Not applicable.

Availability of data and materials

All data generated or analyzed during this study are included in this published article.

Declarations

Ethics approval and consent to participate

The authors declare that they have no competing interests.

Consent for publication

Authors consent the Springer Open license agreement to publish the article.

Competing interests

The authors declare that they have no competing interests.

Received: 3 August 2023 Accepted: 15 September 2023

Published online: 27 September 2023

References

- Lin J, Peng Z, Liu Y, Ruiz-Zepeda F, Ye R, Samuel EL, Yacaman MJ, Yakobson BI, Tour M (2014) Laser-induced porous graphene films from commercial polymers. *Nat Commun* 5:5714. <https://doi.org/10.1038/ncomms6714>
- Ye R, James DK, Tour JM (2019) Laser-induced graphene: from discovery to translation. *Adv Mater* 31:e1803621
- Wang H, Zhao Z, Liu P, Guo X (2022) Laser-induced graphene based flexible electronic devices. *Biosens (Basel)* 12:55. <https://doi.org/10.3390/bios12020055>. <https://www.ncbi.nlm.nih.gov/pubmed/35200316>
- Liu J, Ji H, Lv X, Zeng C, Li H, Li F, Qu B, Cui F, Zhou Q (2022) Laser-induced graphene (LIG)-driven medical sensors for health monitoring and diseases diagnosis. *Mikrochim Acta* 189:54. <https://doi.org/10.1007/s00604-021-05157-6>. <https://www.ncbi.nlm.nih.gov/pubmed/35001163>
- Wan Z, Nguyen N-T, Gao Y, Li Q (2020) Laser induced graphene for biosensors. *Sustain Mater Technol* 25:e00205. <https://doi.org/10.1016/j.susmat.2020.e00205>
- Vivaldi FM, Dallinger A, Bonini A, Poma N, Sembranti L, Biagini D, Salvo P, Greco F, Francesco D (2021) Three-dimensional (3D) laser-induced graphene: structure, properties, and application to chemical sensing. *ACS Appl Mater Interfaces* 13:30245–30260. <https://doi.org/10.1021/acsami.1c05614>
- Zhu J, Huang X, Song W (2021) Physical and chemical sensors on the basis of laser-induced graphene: mechanisms, applications, and perspectives. *ACS Nano* 15:18708–18741. <https://doi.org/10.1021/acs.nano.1c05806>. <https://www.ncbi.nlm.nih.gov/pubmed/34881870>
- Stanford MG, Yang K, Chyan Y, Kittrell C (2019) Tour. Laser-induced graphene for flexible and embeddable gas sensors. *ACS Nano* 13:3474–3482. <https://doi.org/10.1021/acs.nano.8b09622>. <https://www.ncbi.nlm.nih.gov/pubmed/30848881>
- Yang L, Ji H, Meng C, Li Y, Zheng G, Chen X, Niu G, Yan J, Xue Y, Guo S et al (2022) Intrinsically breathable and flexible no(2) gas sensors produced by laser direct writing of self-assembled block copolymers. *ACS Appl Mater Interfaces* 14:17818–17825. <https://doi.org/10.1021/acsami.2c02061>. <https://www.ncbi.nlm.nih.gov/pubmed/35394746>
- Yang L, Zheng G, Cao Y, Meng C, Li Y, Ji H, Chen X, Niu G, Yan J, Xue Y et al (2022) Moisture-resistant, stretchable no(x) gas sensors based on laser-induced graphene for environmental monitoring and breath analysis. *Microsyst Nanoeng* 8:78. <https://doi.org/10.1038/s41378-022-00414-x>. <https://www.ncbi.nlm.nih.gov/pubmed/35818382>
- Huang L, Su J, Song Y, Ye R (2020) Laser-induced graphene: en route to smart sensing. *Nanomicro Lett* 12:157. <https://doi.org/10.1007/s40820-020-00496-0>. <https://www.ncbi.nlm.nih.gov/pubmed/32835028>
- You R, Liu YQ, Hao YL, Han DD, Zhang YL, You Z (2020) Laser fabrication of graphene-based flexible electronics. *Adv Mater* 32:e1901981. <https://doi.org/10.1002/adma.201901981>. <https://www.ncbi.nlm.nih.gov/pubmed/31441164>
- Kaidarova A, Alsharif N, Oliveira BNM, Marengo M, Gerdali NR, Duarte CM, Kosel J (2020) Laser-printed, flexible graphene pressure sensors. *Glob Chall* 4:2000001. <https://doi.org/10.1002/gch2.202000001>. <https://www.ncbi.nlm.nih.gov/pubmed/32257383>
- Wakabayashi S, Arie T, Akita S, Takei K (2020) Very thin, macroscale, flexible, tactile pressure sensor sheet. *ACS Omega* 5:17721–17725. <https://doi.org/10.1021/acsomega.0c02337>. <https://www.ncbi.nlm.nih.gov/pubmed/32715259>
- Wu Y, Karakurt I, Beker L, Kubota Y, Xu R, Ho KY, Zhao S, Zhong J, Zhang M, Wang X et al (2018) Piezoresistive stretchable strain sensors with human machine interface demonstrations. *Sens Actuator A: Phys* 279:46–52. <https://doi.org/10.1016/j.sna.2018.05.036>
- Han T, Nag A, Simorangkir R, Afsarimanesh N, Liu H, Mukhopadhyay SC, Xu Y, Zhadobov M, Sauleau R (2019) Multifunctional flexible sensor based on laser-induced graphene. *Sensors* 19:3477. <https://doi.org/10.3390/s19163477>

17. Yen YH, Hsu CS, Lei ZY, Wang HJ, Su CY, Dai CL, Tsai YC (2022) Laser-induced graphene stretchable strain sensor with vertical and parallel patterns. *Micromachines* 13(8):1220. <https://doi.org/10.3390/mi13081220>
18. Fujita K, Feng Z, Sato D, Kosawada T, Nakamura T, Shiraishi Y, Umezumi M (2018) Modulation of the mechanical properties of ventricular extracellular matrix hydrogels with a carbodiimide crosslinker and investigation of their cellular compatibility. *AIMS Mater Sci* 5:54–74. <https://doi.org/10.3934/matricsci.2018.1.54>

Publisher's Note

Springer Nature remains neutral with regard to jurisdictional claims in published maps and institutional affiliations.

Submit your manuscript to a SpringerOpen[®] journal and benefit from:

- ▶ Convenient online submission
- ▶ Rigorous peer review
- ▶ Open access: articles freely available online
- ▶ High visibility within the field
- ▶ Retaining the copyright to your article

Submit your next manuscript at ▶ [springeropen.com](https://www.springeropen.com)
